PREPRINT. Paper has been published in
Chemical Engineering Journal **64**:1 (1996) 191-197.

Spatio-temporal dynamics in a train of rising bubbles

K. Nguyen[a], C.S. Daw[b], P. Chakka[a], M. Cheng[a], D.D. Bruns[a], C.E.A. Finney[a], M.B. Kennel[a,b]
[a] *University of Tennessee, Knoxville, Tennessee 37996, USA*
[b] *Oak Ridge National Laboratory, Oak Ridge, Tennessee 37831-8088, USA*

Abstract

It has been suggested that rising bubbles in dense fluids resemble an inverted dripping faucet and that they undergo analogous period-doubling bifurcations to chaos. We present experimental results demonstrating that this analogy is weak because the dominant source of instability in the bubble train is inherently different — mutual interactions between spatially separated bubbles as opposed to nozzle dynamics. Unlike the dripping faucet, the initial instability in a bubble train develops at a location far from the injection nozzle and progresses toward the nozzle with increasing gas flow. From both qualitative and rigorous quantitative observations, we conclude that rising-bubble dynamics is best described as "small-box spatio-temporal chaos" with a flow instability. Such dynamics can superficially appear to be simple temporal chaos when considering spatially localized measurements. We show similarity between our experimental results and a bubble-interaction model that accounts for drag and coalescence effects without considering any nozzle dynamics.

Keywords: Bubbling; Chaos; Spatio-temporal systems

1. Introduction

Bubbles are a key element of many basic engineering processes such as boiling, froth flotation, fermentation, fluidization, and gas-liquid extraction. In this study, we focus on understanding the patterns in a simple experiment where bubbles form at the bottom of a narrow container and rise in a single column. We present our experimental results from the perspective of recent developments in nonlinear dynamics. Our principal objective is to show the applicability of low-dimensional and spatio-temporal chaos and explain the most important characteristics of the underlying dynamics and its route to chaos.

Irregular yet clearly non-random dynamic patterns were reported for rising bubbles over 30 years ago [1-4]. At the outset we conjectured that at least some of the irregularities result from deterministic nonlinear processes, motivated by two observations: first, there is some physical similarity between gas bubbles forming in a liquid and liquid drops forming in air; second, a recent model for bubble trains in gas-fluidized beds predicts chaotic behavior [5]. Previous investigators have shown that liquid drops in air (i.e., dripping faucets) clearly exhibit chaotic behavior [6-10], one of the seminal experimental investigations which sparked the modern interest in chaos.

Since we began our investigation [11], others have independently reported period-doubling bifurcations and apparent chaos for gas bubbles in liquids [12,13]. Our study extends earlier experiments in the following ways:

- We make simultaneous measurements of bubble behavior at different spatial locations;
- We use the most recent chaotic signal-processing algorithms to confirm apparent low dimensionality in spatially localized measurements;
- We explain the essential dynamics as arising from a flow instability in the inter-bubble interaction; and
- We show that our experimental observations are consistent with a spatio-temporal model originally derived for bubbles in fluidized beds.

2. Experimental apparatus and procedure

Our experimental apparatus consists of a plexiglass vessel 5×5 cm square in cross section and 26 cm high filled with pure glycerine to a depth of 20 cm [11]. Glycerine is used because of its high viscosity, which reduces bubble-rise rates and increases damping of external vibrations. Air is supplied at a constant flow from a compressed gas cylinder through a pressure regulator, a rotameter, a needle valve (for fine flow control), and a tapered injection tube at the bottom of the column. The air injector is constructed from a 7-mm-O.D. glass tube, tapered at the tip to form a 1-mm-I.D. orifice. An earlier reference [11] explains special details for draining the nozzle that are critical to its proper functioning. Other issues such as moisture absorption and foaming in the glycerine are also dis-

cussed.

Spatially localized dynamics of bubble formation and rise are measured by a pressure transducer located in the air line just prior to the injection nozzle and by two laser beams. The beams are positioned 1.0 and 8.6 cm above the nozzle tip and are monitored by photodetectors. The entire apparatus is mounted on an optical bench supported on air cushions. Both continuous and triggered digitized measurements can be made with the pressure transducer and photodetectors. Continuous measurements are made typically at 500 samples/s, and triggered measurements are made once per bubble.

3. Observed behavior with increasing air flow

As air flow is increased, we typically observe the sequence of patterns shown in Figs. 1a-f. The bubbles formed at the lowest flows are almost perfectly spherical, and they rise from the nozzle with constant inter-bubble spacing (Fig. 1a). As observed at any particular horizontal location (including the nozzle), the measurement signal rises and falls in a simple period-1 fashion as each bubble passes.

Increasing the air flow increases the frequency of bubble formation, and, consequently, the inter-bubble spacing decreases. When the spacing becomes sufficiently small, the inter-bubble spacing is destabilized by the drag-reducing effect of each bubble on its trailing neighbor (Fig. 1b). This destabilization is first visible at the top of the column where alternating trailing bubbles are "drawn" upwards, closing the gap with their leading partner. The upward motion of the trailing bubbles also tends to increase the separation between them and their neighbor below. This "pairing" effect is not initially noticeable at the bottom of the column because the inter-bubble gap takes time to shrink. A measurement made in the upper part of the column (e.g., the upper laser intensity) now produces a signal that appears to have period 2. This change appears to be a bifurcation at the upper location caused by the passage of a slower-faster bubble pair. Near the nozzle, the behavior still appears to be period 1 (at least to the measurement resolution).

When the air flow is increased further, the pairing occurs closer to the nozzle and soon leads to a complete coalescence of the bubble pair into a single larger bubble before reaching the surface. Bubbles in the process of coalescing are distorted (Fig. 1b). Above the coalescence point the single coalesced bubbles again appear to have a period-1 pattern. Horizontal (laser intensity) observations near to and below the coalescence still exhibit a period-2 character.

Increasing air flow moves the coalescence point down further until it reaches the nozzle (Fig. 1c). At this point, the nozzle pressure measurement is clearly period 2. This period-2 pattern persists at the nozzle for higher air flows, while a second pairing and coalescence begins in the upper part of the column (Fig. 1d). This second coalescence pair likewise moves further down with higher air flow until it also occurs at the nozzle. The process is repeated such that we have observed period-4 (Fig. 1e) and period-8 pulsations near the nozzle before the onset of apparent chaos (Fig. 1f).

Here we emphasize some key points about the observations. For spatially localized measurements, such as our laser photodetectors, observed dynamics depend on the location in the column where one is observing because the dissipation in the fluid medium makes the observable effects of spatially dispersed dynamics decay with distance. Measurements near a coalescence of bubbles can show multi-period or even chaotic dynamics; measurements where bubbles are widely spaced are periodic or at least simpler. Bifurcations are observed when an interacting bubble pair moves sufficiently close to a measurement location to be observed by a sensor. Such an observation in an ordinary temporal system would suggest that a fixed point had become unstable, but in our spatially extended system the true bifurcation in the full dynamical system has already occurred.

The initial destabilization begins at the top of the column, opposite from the nozzle. The instability is effectively invisible at the nozzle until increasing air flow moves it sufficiently close to be detected. This behavior is characteristic of spatio-temporal systems, more complicated than simple dynamical systems.

Finally, once a coalescence reaches the nozzle, it continues to persist at higher air flows and is superimposed on succeeding coalescences that move down from above. We have observed this persistence both with video recordings and analysis of time-series measurements made near the nozzle as described in the next section.

4. Analysis of time-series measurements

4.1 Period-doubling transition to chaos

As flow is increased, the measurements at any location appear to exhibit the classic signs of a period-doubling bifurcation to chaos, similar to the dripping faucet [14,15].

Time-series measurements from the lower laser corresponding to period-1, period-2, period-4, and aperiodic bubbling are depicted in Figs. 2a-d. For all time-series plots, the ordinate is scaled to the greatest peak-to-trough difference in each plotted time segment,

and reported flows are normalized to the first period-doubling bifurcation in the pressure signal. At low flow, when pairing is not near the measurement location, the signal rises and falls periodically over time (Fig. 2a). For laser measurements, the rise and fall of the signal corresponds to a bubble passing through the beam. In the period-1 condition, all bubbles and their signals are identical to within the measurement resolution.

As air flow is increased and the bubble-coalescence location moves closer to the measurement locations, the signals develop two distinct peaks, one corresponding to leading bubbles and one to trailing bubbles (Fig. 2b). The time intervals between peaks alternate between short and long, the shorter one resulting from the acceleration of a trailing toward a leading bubble.

Two sequential coalescences near the measurement location at still higher flow result in repeating sequences of four distinct events (Fig. 2c). The signal for the apparently aperiodic case (Fig. 2d) confirm the nonrepeating nature of the bubble sequences above the critical flow.

The upper-laser signal displays different sequences, as shown in Fig. 3a-d. The signal for low air flow exhibits a single periodic peak corresponding to the passage of large identical bubbles (Fig. 3a). As air flow is increased, the first coalescence begins near the top of the column, evident in a period-2 signal (Fig. 3b). Visual observations indicate that the location of the coalescence point continually shifts over time, possibly due to the disturbance produced by bubbles breaking at the nearby liquid surface.

At still higher air flow, the location of the first coalescence migrates toward the injection nozzle, and the upper laser beam is affected only by the passage of previously coalesced bubbles. The resulting signal appears to be a noisy period-1 pattern (Fig. 3c). This transition from noisy period 1 to unstable period 2 back to noisy period 1 appears to repeat with the onset and migration of the second coalescence with more air flow increases. The pattern at the upper beam finally appears to jump rapidly to aperiodicity when the critical flow is reached and surpassed (Fig. 3d).

Time return plots of the pressure measurements for four distinct regions of periodicity are shown in Fig. 4a-d. Each plot axis represents the Nth and $N+1$th time interval between successive crossings of the pressure-signal mean value. The collection of points produced by plotting successive pairs of time intervals in the pressure data create a "map" that characterizes the behavior of the bubbling over time. When start-up transients are excluded from consideration, the resulting point patterns are referred to as "attractors".

The time intervals between bubbles form maps of 1, 2, 4 and 8 points, each of which represents a periodic mapping of a fixed point, as air flow is increased from the single-bubble condition at low flow. Figures 4a-b show example period-4 and period-8 maps.

Aperiodic bubbling produces a more complex return plot, such as the example shown in Fig. 4c. In this case, the successive return points seem to define a curved region of the plot but never exactly repeat. The layered appearance of the mapping region is consistent with the fractal structure produced by deterministic chaos when it occurs in dissipative systems. There appears to be qualitative similarity between this pattern and patterns reported for the dripping faucet [6-10].

An interesting feature of the period-4 (Fig. 4a) and period-8 (Fig. 4b) maps is the apparent "fuzziness" of the time intervals. We observe that the fuzzy regions around these points are not obviously random but rather suggest that there is a partial filling-in of the attractor that emerges more completely at higher flows (Fig. 4c). We conjecture that this is the result of dynamic noise; i.e., small-amplitude dynamics which couples with the main bubble dynamics as opposed to measurement noise, which would have a more symmetric distribution. This effect is especially visible in Fig. 4d, which depicts a noisy period-4 window at a dimensionless flow of 3.9 (well above the critical flow for onset of chaos). We have observed similar effects when dynamic noise is added to numerical models such as the logistic map. Such noise could possibly come from either the experimental surroundings (e.g., in the form of mechanical vibrations) or, more interestingly, the spatio-temporal nature of the bubble column. We discuss this second possibility below.

4.2 Time series algorithms: dimensionality, entropy and nonlinearity

We confirm the apparent observation of low-dimensional chaos with recent time series algorithms. We estimate the correlation dimension and Kolmogorov entropy of the pressure signals to quantify the changes that occur as air flow changes. Both of these quantities are measures of relative signal complexity.

Our estimation procedures use methods suggested by Takens [16] and Schouten *et al*. [17,18]. These determine correlation dimension and Kolmogorov-Sinai entropy with a maximum-likelihood principle and provide confidence limits on the results. As described by the references, it is necessary to specify an appropriate embedding time window and an upper length scale for determining maximum-norm separations between trajectory segments (i.e., points on the

embedded trajectory). The embedding lag is set to one sampling interval. In our implementation, we select an embedding window on the order of the longest period in each time series. This length is somewhat longer than that recommended by Schouten *et al*. [17], but we have found it to be more effective for nearly periodic data. We choose an upper length scale equal to the absolute deviation of each time series from its mean, the same as used by Schouten *et al*.

Our correlation-dimension and entropy estimates are depicted in Fig. 5. The entropy values are reported in bits per cycle, where a cycle is defined by successive upward crossings of the signal mean value and corresponds to the interval between successive bubble formations. For the period-1 through period-4 regions, correlation dimension stayed close to one with a slight elevation above one that we attribute to noise. Likewise, entropy remained essentially at zero for this region. Both of these values (one and zero, respectively) are consistent with periodic (either single or multiple) behavior. For air flow above the critical, correlation dimension increased rapidly above two, and entropy (sum of positive Lyapunov exponents) increased to a significant positive value, both consistent with an onset of chaos. A dip in dimension and entropy between dimensionless flows of 3 and 4 corresponds to an apparent periodic window.

We employ the "method of surrogate data" [19] in order to test whether the data in the aperiodic state exhibit nonlinear characteristics or if any observed autocorrelation results from a simpler relationship, namely linearly correlated noise. The phases of the Fourier transform of the original data are randomly shuffled and the inverse transform is applied to generate a surrogate time series that has the same autocorrelation as the original. We also rescale the surrogates to have the same distribution as the original series.

To test the null hypothesis that the data have no structure beyond merely linearly correlated noise, the original and surrogate series are compared with discriminating statistics. If the data had been nonlinear, then the phase-randomization process will have destroyed important information, and the statistical values will differ significantly. We choose two statistical methods: the method of false nearest neighbors (FNN) and the bivariate mutual information function (described in the next section). The method of FNN [20] is a well-established technique to help determine the minimum embedding dimension needed to reconstruct the phase-space trajectory of a time series. As the minimum embedding dimension is reached, the fraction of FNN should converge, and this minimum embedding dimension can provide an upper-bound estimate of the topological dimension of the phase-space attractor. We implement an improved version of this test, "false nearest strands" (FNS) [21], which corrects for errors due to temporal oversampling, autocorrelation, and sparse regions in phase space.

We generate multichannel surrogates [22] of the three simultaneously measured signals at a dimensionless flow of 4.6 (see Fig. 2d,3d). The multichannel surrogates preserve both autocorrelation and crosscorrelation relationships. A comparison using FNS of the original and surrogate pressure series for a range of embedding dimensions and delays is shown in Fig. 6. The statistical values for the original and surrogate data are significantly different, rejecting a null hypothesis of linearly correlated noise and suggesting nonlinear structure in the data. Additionally, the converged finite fraction at low dimension and lag suggests authentic low dimensionality. This is a stronger statement than merely nonlinearity, which is all that the rejection of the surrogate data class implies.

4.4 Spatio-temporality

It is clear from the above results that the dynamical features one observes depend on measurement location, suggesting that the bubble column is a spatio-temporal system [11,14]. Events that occur near a measurement point (e.g., a nearby coalescence) can be readily detected, whereas information about distant events (e.g., a coalescence at the opposite end of the column) can be damped to the measurement threshold and thus become effectively invisible. The alternative — which we reject — is dynamics dominated by nozzle effects, where bubbles are emitted chaotically, but rise thereafter without interaction, which best describes the dripping faucet. We find essential dynamics to be entirely different in chaotic bubbling, despite the superficial physical analogy and similar time series behavior. We have never observed anything but completely periodic bubbling when there was only one bubble in the column, and thus nothing to interact with.

Previous researchers [23,24] have characterized the spatio-temporal behavior of complex fluidized beds using spatial entropy, a measure of information loss between measurement locations. We choose a related measure, the bivariate mutual information function, to quantify shared information between locations. The mutual information function [25] has become a standard tool in chaotic time series analysis, and the bivariate mutual information function has been demonstrated as a useful tool to measure spatial coupling in fluidized beds [26]. For a spatio-temporal system, the degree of coupling is expected to decrease with distance.

Figures 7a-b show the mutual information between

the lower-laser and injection-pressure signals and between the upper-laser and injection-pressure signals. Also plotted are mutual information functions for the corresponding surrogate series. As is clearly seen in these plots, the degree of coupling between a location in the column and the injection nozzle decreases with distance. This degradation of information with increasing spatial separation is consistent with spatio-temporal dynamics occurring inside the full length of the bubble column during the propagation of the bubbles; information loss may be attributed to coalescences between measurement locations. On the other hand, the mutual information between the surrogate series is significantly less than that between the original series, implying that there is still in fact some real dynamical coupling between the signals, ruling out measurement artifacts. We infer from these plots and the results of the previous section that the bubble column is a fairly low-dimensional but nevertheless spatio-temporal chaotic system.

We have observed that the "fuzziness" in the return maps described earlier is independent of the isolation of the apparatus from its surroundings. We have tested this by removing the air cushion from the optical bench supporting the bubble column; no change was seen. On this evidence and our model, we conjecture that the dynamic "noise" is not random but a result of other dynamics propagating from elsewhere in the column. At a large length scale (in state space) one sees only the simple dynamics of the local low-dimensional interactions, but at smaller and smaller length scales the effects of more distant dynamics become more apparent. The blurring of bifurcations and premature appearance of chaotic structure are general characteristics of spatio-temporal systems: distant spatial locations with their own dynamics are coupled to the observation point to some degree. If the bubble column were infinite in physical height, we might theoretically see unlimited layers of complexity as we went to smaller and smaller length scales, a feature common to spatio-temporal systems but not conventional low-dimensional dynamical systems. The proportion of false strands converged to a non-zero "noise" plateau for most data runs, but we feel that this apparent noise is in fact unresolved smaller-scale dynamics added on to the dominant low-dimensional behavior.

We suggest that our bubble column is an especially simple example of spatio-temporal chaos that may provide insights into the nature of such systems. Unlike many examples of spatio-temporality, the bubble column exhibits relatively low-dimensional gross behavior that is conducive to fundamental understanding. The system is less complicated than fully chaotic spatio-temporal continuum partial differential equations, because the interesting dynamics are mostly lumped around discrete bubbles.

5. Comparison with the Daw-Halow bubble model

A dynamical model for bubble behavior in fluidized beds was recently proposed by Daw and Halow based on experimental observations of bubble interactions [5]. The model is a set of nonlinear, ordinary differential equations, each equation representing the time rate of change of the vertical position for a given bubble. The velocity of each bubble is determined by its size as well as its proximity to the bubble just above it. This latter feature is represented as an empirically determined power-law relationship.

From a mathematical point of view, this model is somewhat unusual in that the number of differential equations equals the number of bubbles, and this number changes with time due to bubbles coalescing or exiting the top. Despite this complexity and despite the differences between fluidized beds and liquids, we believe this model is useful for understanding the bubble column because it is constructed to represent the same basic physical configuration, a single column of vertically rising bubbles. For our discussion here, the model parameter values reported here are identical with those suggested in [5], except that the physical dimensions of the bed have been changed to 20 cm in height and 5.7 cm in diameter, and a constant bubble diameter of 1.2 cm has been used. The rate of gas injection is then determined by specifying the bubble injection frequency.

In comparing this model with our experimental bubble-column observations, the most prominent similarity is in the bubble-pairing (bifurcation) phenomenon. As described in [5], the model predicts the onset of pairing and coalescence as bubble-injection frequency increases. In the moving frame of the bubbles, a state of constant separation becomes unstable beyond a certain flow rate.

The model also shows each pairing and coalescence zone moving down toward the nozzle as the bubble injection rate increases, and it predicts a period-doubling bifurcation sequence associated with these coalescences prior to the onset of aperiodic behavior. All of the above suggests good agreement between the model and experiment up to the critical flow.

Figure 8 is a two-dimensional time return map predicted by the model for aperiodic bubbling just beyond the critical injection rate. This map bears some similarity to the corresponding experimental plots shown above. We do not mean to imply that the detailed behavior of the model exactly matches our experiment,

but there do appear to be important similarities even above critical flow, and we believe that the model captures the inter-bubble interaction essential for chaos in the bubble column.

Beyond the critical air flow, we also observe that the model predicts the occurrence of periodic windows. This is consistent with our experimental observations and also consistent with behavior reported for the dripping faucet [6-10]. Finally, because of spatio-temporality the model also exhibits the same dynamical fuzziness in what would otherwise be clean low-dimensional time traces.

6. Conclusions

For our column, flow instabilities leading to bifurcations and chaotic dynamics are dominated by inter-bubble interactions that depend primarily on bubble spacing. The Daw-Halow model incorporates empirically determined inter-bubble relationships, and although developed to describe a different gas-fluid system, it mimics the behavior of our experimental system. As the dripping-faucet system has been shown to be dominated by drop and flow dynamics locally at the faucet outlet, the analogy between a stream of falling droplets and a train of rising bubbles is weak.

The spatial dependence of the bubble-train dynamics is reflected in differences between simultaneous local measurements. The system behavior may described as small-box spatio-temporal chaos, as local measurements exhibit temporal chaotic dynamics which appears low dimensional due to information attenuation below the measurement threshold.

Acknowledgements

This work was partially funded by the U.S. Department of Energy, Morgantown Energy Technology Center.

References

[1] F.W. Helsby and K.R. Tuson, (based on work performed at Admiralty Laboratory, Holton Heath, Dorset, United Kingdom), *Research*, *8* (1955) 270-275.

[2] K.R. Tuson, *Br. J. Appl. Phys.*, *6* (1955) 99-100.

[3] J.F. Davidson and B.O.G. Schüler, *Trans. Inst. Chem. Eng.*, *38* (1960) 144-154.

[4] L. Davidson and E.H. Amick Jr., *AIChE Journal*, *2* (1956) 337-342.

[5] C.S. Daw and J.S. Halow, *AIChE Symposium Series*, No. 289 (1992) 61-69.

[6] R. Shaw, *The Dripping Faucet as a Model Chaotic System*, Aerial Press, Santa Cruz, California, 1984.

[7] P. Martien, S.C. Pope and R.S. Shaw, *Phys. Lett. A, 110* (1985) 399-404.

[8] X. Wu and Z.A. Schelly, *Physica D, 40* (1989) 433-443.

[9] R.F. Cahalan, H. Leidecker and G.D. Cahalan, *Comput. Phys.*, *4* (1990) 368-383.

[10] K. Dreyer and F.R. Hickey, *Am. J. Phys.*, *59* (1991) 619-627.

[11] P. Chakka, *M.S. Thesis*, University of Tennessee, Knoxville, 1994.

[12] D.J. Tritton and C. Egdell, *Phys. Fluids A, 5* (1993) 503-505.

[13] L.J. Mittoni, M.P. Schwartz and R.D. La Nauze, *Phys. Fluids*, *7* (1995) 891-893.

[14] F.C. Moon, *Chaotic and Fractal Dynamics*, Wiley, New York, 1992.

[15] S.H. Strogatz, *Nonlinear Dynamics and Chaos*, Addison-Wesley, Reading, Massachusetts, 1994.

[16] F. Takens, in *Dynamical Systems and Bifurcations*, Lecture Notes in Mathematics, Springer-Verlag, Berlin, *1125* (1984) 99-106.

[17] J.C. Schouten, F. Takens and C.M. van den Bleek, *Phys. Rev. E, 49* (1994) 126-129.

[18] J.C. Schouten, F. Takens and C.M. van den Bleek, *Phys. Rev. E, 50* (1995) 1851-1861.

[19] J. Theiler, S. Eubank, A. Longtin, B. Galdrikian and J.D. Farmer, *Physica D, 58* (1992) 77-94.

[20] M.B. Kennel, R. Brown and H.D.I. Abarbanel, *Phys. Rev. A, 45* (1992) 3403-3411.

[21] M.B. Kennel and H.D.I. Abarbanel, preprint available at ftp://angst.engr.utk.edu/pub/preprints/fns.tar.gz.

[22] D. Prichard and J. Theiler, *Phys. Rev. Lett.*, *73* (1994) 951-954.

[23] M.L.M. van der Stappen, J.C. Schouten and C.M. van den Bleek, *Proceedings, 1st International Particle Technology Forum*, AIChE (1994) 446-451.

[24] M.L.M. van der Stappen, J.C. Schouten and C.M. van den Bleek, *Fluidization VIII* (1995).

[25] A.M. Fraser and H.L. Swinney, *Phys. Rev. A, 33* (1986) 1134-1140.

[26] C.S. Daw and J.S. Halow, *AIChE Symposium Series*, No. 296 (1993) 103-122.

Figures

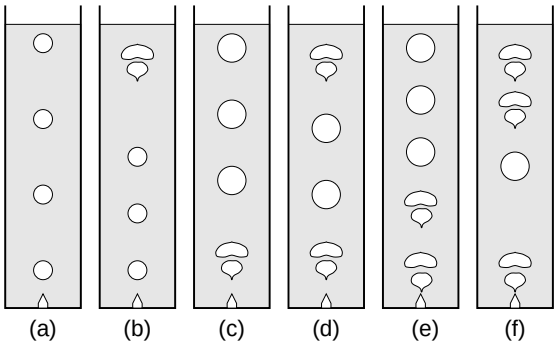

Fig. 1. Progression of bubble-train complexity with flow, from simple periodic at low flow (a) to multi- or aperiodic at higher flow (f).

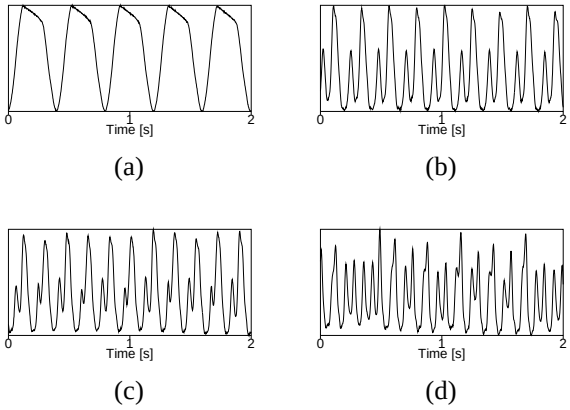

Fig. 2. Example time series of lower-laser beam attenuation for dimensionless flows of (a) 0.25, (b) 1.5, (c) 2.05 and (d) 4.6.

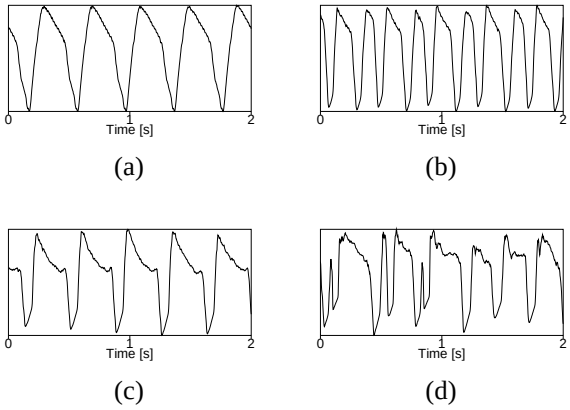

Fig. 3. Example times series of upper-laser beam attenuation for dimensionless flows of (a) 0.25, (b) 1.7, (c) 1.9 and (d) 4.6.

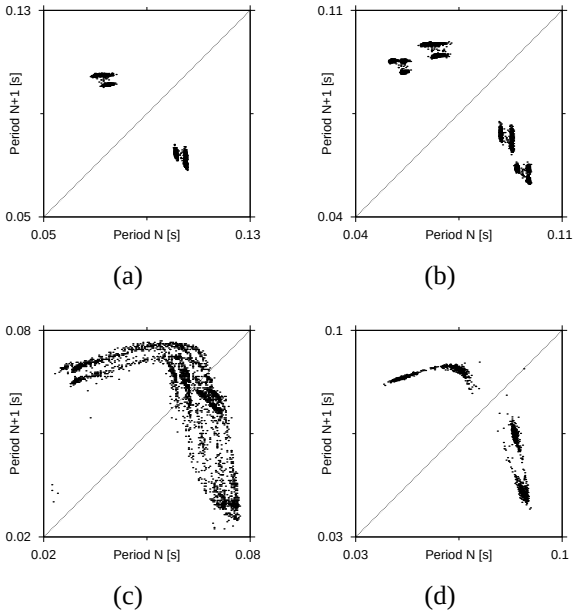

Fig. 4. Example two-dimensional time return maps for the injector pressure as air flow is increased for dimensionless flows of (a) 1.8, (b) 2.2, (c) 4.9 and (d) 3.9.

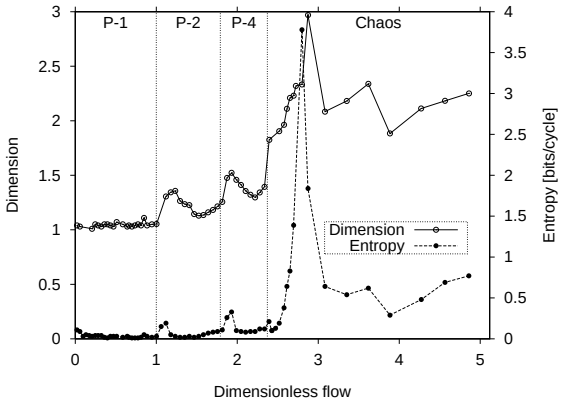

Fig. 5. Variation of pressure-signal dimension and Kolmogorov entropy with air flow.

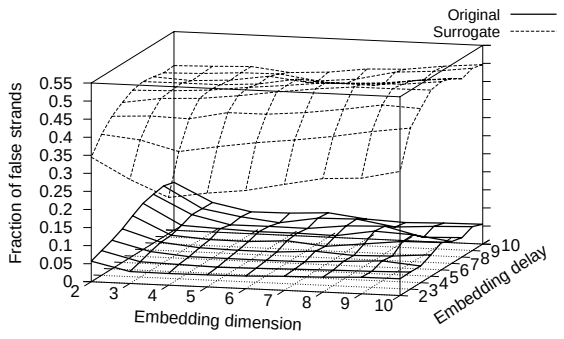

Fig. 6. Fraction of false nearest strands for original and surrogate time series for a dimensionless flow of 4.6.

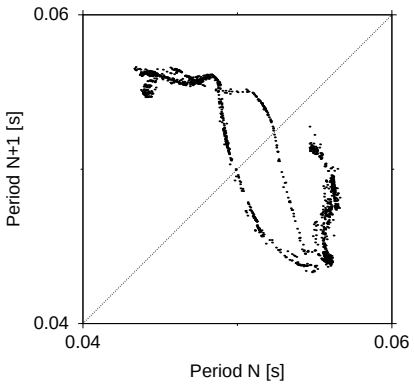

Fig. 8. Example time return map from Daw-Halow
model in the chaotic regime.

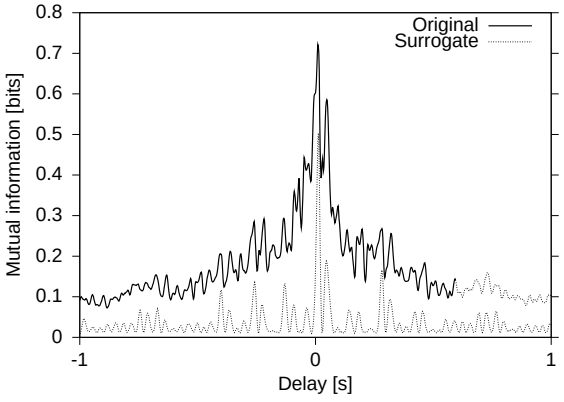

(a)

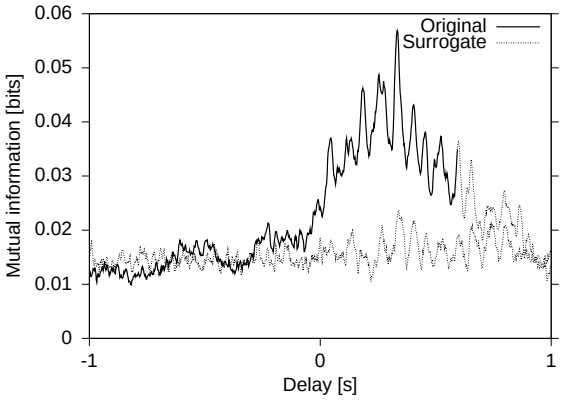

(b)

Fig. 7. Mutual information for lower-laser with respect to pressure signal (a) and upper-laser with respect to pressure signal (b) at dimensionless flow of 4.6.